

Variability of Radar Reflectivity in Continental Boundary Layer Stratocumulus

Aaron M. Botnick

*National Weather Center Research Experiences for Undergraduates, Norman, Oklahoma
University of Louisiana at Monroe, Monroe, Louisiana*

Yefim L. Kogan and David B. Mechem

*Cooperative Institute for Mesoscale Meteorological Studies
University of Oklahoma, Norman, Oklahoma*

Last Revised:

August 12, 2005

Corresponding Author Address:

Aaron M. Botnick

129 Cottage Dr.

Luling, LA 70070

botnicka@cox.net

(504) 508-2355

Abstract

Boundary layer stratocumulus clouds play an important role in the Earth's radiative budget and climate. This paper uses reflectivity data from the Millimeter-Wave Cloud Radar (MMCR) at the Southern Great Plains (SGP) Atmospheric Radiation Measurement Climate Research Facility (ACRF) to explore variability of continental boundary layer stratocumulus. Neglecting subgrid variability in numerical models can lead to biases in radiative heating and microphysical process rates. Analysis of over 70 hours of radar data demonstrates that cloud system variability increases with mean reflectivity, indicating that drizzling clouds are more variable than nondrizzling clouds. Variability is highly vertically dependent, suggesting that numerical model accuracy may improve if this vertical dependency is included in subgrid cloud parameterizations.

1. Introduction

The important role of marine stratocumulus clouds in climate and numerical weather prediction is well recognized. It is frequently shown that an increase in stratocumulus cloud cover of only a few percent would compensate for greenhouse warming due to CO₂ doubling, while a similar decrease would double the warming (e.g., Randall et al. 1984; Ramanathan et al. 1989). Clearly, even a relatively small bias in stratocumulus representation in mesoscale or global circulation models may result in serious errors in the simulated regional weather and global climate predictions.

Continental stratocumulus are no less important, however, they have been studied less frequently. This study focuses on one particular aspect of continental stratocumulus characterization, namely a description of their variability in both the horizontal and vertical directions. Numerous studies have shown that neglecting variability at scales smaller than model

grid (subgrid variability) can lead to substantial biases in radiative quantities (e.g., Cahalan et al. 1994), as well as microphysical process rates (e.g., Kogan 1998; Rotstayn 2000; Pincus and Klein 2000; Larson et al. 2001a; Wood et al. 2002).

Variability is typically characterized by probability distribution functions (PDFs). The most straightforward way to define a PDF is to assume that it can be represented by a known analytical function. For example, a two-parameter Gaussian function with the first parameter (mean value of the parameter) predicted by the model and the second parameter (standard deviation) defined by some parameterization or closure (e.g., Larson et al. 2001b; Price 2001; Larson et al. 2002; Price and Wood 2002; Kogan et al. 2005).

Studies suggest that standard deviation depends strongly on cloud type, presence of precipitation, and the model grid size (e.g., Kogan et al. 2005). It is, however, unknown if variability (standard deviation) has a significant vertical dependence. If the latter can be neglected, then a universal PDF with a constant standard deviation could be employed to characterize variability in the whole cloud layer, and the formulation of subgrid variability in numerical models would be simplified. The vertical dependence of variability will be the focus of this study.

Cloud variability was evaluated based on radar reflectivity data collected by the Atmospheric Radiation Measurement program (ARM) (Stokes and Schwartz 1994). Since September of 1996, the Southern Great Plains (SGP) ARM Climate Research Facility (ACRF) has operated a Millimeter-Wave Cloud Radar (MMCR) capable of detecting small cloud droplets (Moran et al. 1998). Determination of cloud base and height were made using a combination of the SGP ACRF's lidar and ceilometer (Clothiaux et al. 2000), as radar data were not reliable for this purpose, especially when virga or insects were present. These data were compiled in the

Active Remote Sensing of Clouds (ARSCL) Value Added Product (VAP) discussed in section 2a.

The layout of this paper is as follows. Section 2 describes the data source, instrumentation, and general dataset information. Section 3 covers the methodology used in analysis of the data. Section 4 outlines the results of the study and continues with a discussion of these results. A summary and conclusions follow in section 5.

2. Data

a. ARSCL Value Added Product

The Active Remote Sensing of Clouds (ARSCL) Value Added Product (VAP) contained MMCR reflectivity data and estimated cloud boundaries (Clothiaux et al. 2000). Data streams used during data assimilation and segmentation were cloudBaseBestEstimate, cloudTopBestEstimate, and reflectivity data as a function of height. The cloudBaseBestEstimate was determined by the method of Clothiaux et al. (2000) and used the laser ceilometer and the Micro Pulse Lidar (MPL) for clouds below 3km. It should be noted that this dataset contained clouds with tops less than 1500 m. Cases were identified by analyzing data from Professor Jay Mace's ARM Archive (<http://www.met.utah.edu/mace/homepages/research/archive/sgp/sgp.html>). Data from the MMCR merged moments imagery were used for the initial query. Section 3a covers the segmentation of cases in detail.

b. Instrumentation

The primary source of data for this study is the MMCR. This radar points vertically and operates at 35 Ghz with an 8.77 mm wavelength (K_a band). This short wavelength enables it to

discriminate small cloud droplets and other nonhydrometeor objects. This instrument has an operational range of 10-30 km; however, ARM data uses a ceiling of 14 km. Beyond that range, or in moderate precipitation, the radar beam is attenuated. With its short wavelength and no need for scanning strategies, the effective beamwidth for this radar is 0.2° - 0.3° . This beamwidth gives the radar a range resolution of 35-50 m, which is significantly higher than the WSR-88D radar, ~1000 m (Moran et al. 1998). The ARSCL VAP uses a vertical gate spacing of 45 m. While the MMCR is a Doppler radar, only the reflectivity data are used in this study.

The ARSCL VAP incorporates measurements from two laser instruments, the MPL and Belfort Laser Ceiliometer or Vaisala Ceiliometer (BLC or VCEIL), to detect cloud boundaries with higher accuracy than the MMCR alone. The BLC uses a 910 nm laser with a range of 7.3 km and vertical resolution of 7.6 m (Flynn 2004a). The VCEIL replaced the BLC in the summer of 2000. The VCEIL uses a 905 nm laser with a range of 7.5 km and a vertical resolution of 15 m (Flynn 2004b). The MPL uses a 523.5 nm laser that has a maximum vertical range of 18 km depending on the cloud thickness. The MPL has a vertical resolution of 30 m and these measurements are averaged every 30 seconds (Flynn 2005).

c. Dataset

This study analyzed 70.4 hours of boundary layer stratocumulus observations over the SGP ACRF during the 1998 to 2003 period. This relatively small dataset was obtained by applying a very strict data quality control and narrowly focused selection criteria with respect to cloud type and mesoscale variability. This process is described in more detail in the following methodology section. The analyzed stratocumulus clouds were typically associated with frontal passages during the winter months, from November through early March. Data for each day were further segmented to approximately 0.5-1.5 hours or 18-54 km, assuming cloud motion of

10 m s^{-1} . The distribution of data segment lengths is shown in Figure 1. About 40% of the segments have durations in the 0.5-1 hour range, while 57% are in the 1-1.5 hour range.

New near-field corrections were required for MMCR data below 1000 m, as the old corrections were found to contain errors. These corrections were especially important below 500 m AGL, where many of the subcloud and base observations were located. At the time of this study, the archived data had not been reprocessed to reflect these corrections. Therefore, these corrections were applied during the data processing stage of this study.

3. Methodology

a. Segmenting

Most of the boundary layer segments over the SGP ACRF during the analyzed winter seasons occurred under a strong inversion located at about 900 mb. The boundary layer clouds were often overlaid by cumuliform clouds and/or a cirrus deck. A preliminary dataset was compiled using the low-level merged moments imagery. The multiple layer cloud systems were included in the analysis, as long as no precipitation shafts interfered with the stratocumulus clouds.

The first step in applying a quality control scheme was to reduce contamination in the dataset due to insects and other nonhydrometeor targets. These targets are often referred to as “atmospheric plankton” by Lhermitte (1966). The problem is especially difficult in the spring and summer seasons and less severe during the analyzed winter season. Discrimination between contaminated and clean data was achieved through examination of the top and base height estimates along with radiometer data. If the radar showed high reflectivity and the direct beam solar irradiance measurement showed values associated with clear skies, then the case was deemed to be contaminated, and removed from the dataset. As well, if the estimated cloud

boundaries were missing or seriously in error (e.g. cloud base higher than cloud top), the case was removed. Profiles with maximum reflectivity below -50 dBZ were also rejected from analysis.

After the initial segments were compiled, the data were sent through a custom data extraction program. Variability of the radar data were examined at four levels: subcloud, base, middle, and top. The subcloud layer was defined to be 3 range gates, or 135 m, below the base layer. The base layer was defined as the average of all ARSCL VAP base heights in the segment. The top layer was defined as the lowest top height identified by the ARSCL VAP, while the middle layer was the average between the top and base heights. The program then extracted and printed a file containing the reflectivity values over the time domain at each of the four levels. Next, a mean reflectivity was calculated for each of the four layers per segment, along with the standard deviation of each layer. A separate file was created for the entire dataset, consisting of the mean layer variability data for the four layers.

After preliminary segmentation of the dataset had taken place, a second pass of the data was completed. The second pass analyzed each case based on their top and bottom heights. As this study looked at radar reflectivity, the segments were then subdivided into 0.5-1.5 hour segments keeping the top height nearly constant to minimize mesoscale variability. Segments were further subdivided if the base height varied more than 20%. The program also removed data where mean layer reflectivity was < -50 dBZ; if the resulting segments did not contain enough data, they were removed from the dataset. Segments found still containing mesoscale variability were also removed from the dataset. These revised segments were then passed through the program again to re-compute the heights at the four levels, their mean reflectivity values, and standard deviations.

b. *Statistical Definitions*

The dataset comprised 66 segments and 70.4 hours of clean data. Figure 1 shows the distribution of the data, where most of the data is centered around a 1 hour segment length. The first step calculated the reflectivity mean and standard deviation at each of the four levels.

Horizontal standard deviation will hereafter be referred to as the Cloud Variability Parameter (CVP). The reflectivity at a given time or horizontal position is denoted as Z_i and the mean

reflectivity at one level will be represented as: $\bar{Z} = \sum_{i=1}^n (Z_i) / n$. The CVP at one level is σ , and

will be defined as:

$$\sigma = \left(\sum_{i=1}^n (Z_i - \bar{Z})^2 / n \right)^{1/2} \quad (1)$$

To differentiate σ between layers, the notation σ_j will be used, where $j = \{1, 2, 3, 4\}$. The subcloud CVP will be denoted as σ_1 and σ_4 will refer to the cloud top CVP. For analysis of the CVP vertical dependence, we introduce the Vertical Variability Parameter (VVP). The VVP is denoted by the letter δ and defined as the standard deviation of the four CVP values as:

$$\delta = \left(\sum_{j=1}^m (\sigma_j - \bar{\sigma})^2 / (m - 1) \right)^{1/2} \quad (2)$$

In (2) $\bar{\sigma}$ denoted the mean value of the CVP over all four levels:

$$\bar{\sigma} = \sum_{j=1}^m (\sigma_j) / m \quad (3)$$

4. Results and Discussion

a. *Cloud Variability Parameter*

In the plots shown below, the CVP is plotted versus the mean subcloud reflectivity; the latter is closely related with the amount of drizzle below a cloud. As Fig. 2 shows, standard deviation in general increases with subcloud reflectivity. As larger values of subcloud reflectivity may indicate the presence of drizzle, it may be inferred that drizzling clouds exhibit larger reflectivity. The distinction between drizzling and nondrizzling clouds was made by applying a threshold reflectivity value identified in a number of previous studies. Sauvageot and Omar (1987), Wang and Geerts (2003) suggested a threshold value between -20 and -15 dB. Mace and Sassen (2000) found that continental clouds at the SGP ACRF with reflectivities > -20 dBZ had a high probability of drizzling. Kogan et al. (2005), also in the study of boundary layer clouds over the SGP ACRF, provided arguments for a reflectivity threshold of -17dBZ as a good estimation of a drizzling state. By using the -17 dBZ threshold, it was found that the mean CVP for cloud segments with mean subcloud reflectivity (Z_{sc}) less than -17 dBZ was about 1.8 dBZ, while cloud segments with $Z_{sc} > -17$ dBZ had a mean CVP of 2.5 dBZ. It can also be inferred that the nondrizzling clouds tend to be more homogenous than their drizzling counterparts, as the CVP of the four layers were much closer, whereas the drizzling clouds had drastically different CVP values. This is clearly shown in the vertical range of data for drizzling and nondrizzling clouds in Fig. 2. Nondrizzling clouds have a smaller range, showing similar variability in all layers. The drizzling clouds show the opposite behavior, with larger ranges in the CVP between layers. Figure 2 also shows that most of the nondrizzling segments were clustered around -38 to -28 dBZ, while drizzling segments clustered around -15 to -3 dBZ.

Figure 3 shows the four layer CVP values against the mean subcloud reflectivity, Z_{sc} . Data for each layer are shown in separate plots, easing analysis of each layer's variability. Added to Figure 3 are third order polynomial curve fits for each layer, allowing trends to be more easily seen. All layers displayed a similar trend of increasing variability following the increase in mean subcloud reflectivity. The top layer showed a pronounced region of higher variability, along with a much faster increase as compared to other layers. A notable feature in the layers below cloud top is the presence of a local maximum around -15 dBZ. Given the rather small size of this dataset, it was difficult to conclude whether this feature represented real smoothing of cloud fields as precipitation increases, or just an artifact of insufficient data at the right end of the analyzed data range.

The curve fits shown in Figure 4 confirmed that the top layer had significantly higher variability than the other layers. The CVP in the top layer increased from 2.5-3.0 dBZ for nondrizzling cloud segments, to 3.5-4.0 dBZ for drizzling cloud segments. In the other three layers, CVP varied from 1.2-1.8 dBZ for nondrizzling cloud segments, to 1.8-2.8 dBZ in drizzling segments. The interesting merge and then steady decline in CVP between the subcloud and base layers might suggest the existence of a local maximum near -15 dBZ may not be an anomaly of curve fitting or an artifact of small sampling, but rather related to the drizzle process. Figure 5 is similar to Fig. 2 in displaying the CVP versus the mean reflectivity; however, Fig. 5 shows the CVP versus the reflectivity at each level. This enables one to see that reflectivity at the top of the cloud only reaches the -17 dBZ threshold for 7 out of the 66 segments. Most of the top layer values correspond to small cloud drops and, hence, have relatively small reflectivity. Larger values of reflectivity in the subcloud and base data indicated the presence of larger cloud drops in this region.

b. *Vertical Variability Parameter*

Thus far, it has been shown that the top layer is significantly more variable than the lower layers of these clouds through analysis of the CVP. The difference in variability at different levels can be more clearly illustrated using the vertical variability parameter (VVP), δ . Figure 6 shows $\bar{\sigma}$ along with bars representing δ , or the standard deviation of $\bar{\sigma}$. The δ parameter conveniently illustrates the spread among the four CVP values. The trend in the $\bar{\sigma}$ data is similar to the one previously found in the horizontal data where the variability increased with an increase in reflectivity. The larger the bars in this figure, the more variable the cloud is in the vertical. For example, the cloud segments in the -38 to -28 dBZ range tended to have much smaller vertical variability when compared with drizzling segments. The nondrizzling cloud segments were much more homogeneous in the vertical; thus, there is a much stronger vertical dependence for drizzling clouds than for nondrizzling clouds.

Another way to visualize these changes is to look at the number of segments containing a minimum or maximum in variability at a given layer. Figure 7 shows that the highest number of maximum standard deviations is in the top layer. This coincides nicely with all the previous data suggesting that the top of the cloud is the most variable, especially when the minimum standard deviation occurrences are by far the lowest of the four layers. These data also suggest that the middle layer can be considered nearly homogeneous, as it varies the least of any layer. The subcloud layer was the most variable of the lower layers. It is interesting to note that the minimum and maximum standard deviations are nearly the same in the subcloud layer.

5. Summary and Conclusions

Data were collected from the SGP ACRF from 1998 to 2003 consisting of clean boundary layer stratocumulus segments. The dataset comprises 66 segments of lengths ranging from 0.5-1.5 hours, resulting in 70.4 hours of analyzed data. These data were analyzed for horizontal variability using the cloud variability parameter (CVP) defined as mean segment standard deviation. Vertical variability was analyzed using the vertical variability parameter (VVP), defined as the standard deviation of the four CVP values. Overwhelmingly, the results showed a strong vertical dependence in these clouds. Of the four layers analyzed, the top layer displayed the highest variability. This ranged from 2.4-4.0 dBZ, rising steadily as reflectivity was increased in the subcloud layer, following a change from nondrizzling to a drizzling state. The subcloud layer had the second highest variability, ranging from 1.8 dBZ to a local maximum of 2.7 dBZ at the drizzle threshold of -17 dBZ. This variability then fell steadily to 1.6 dBZ as reflectivity increased. The base and middle layers of the cloud showed similar trends to that of the subcloud layer. Nondrizzling segments had the smallest vertical variability; the vertical variability of drizzling segments was approximately 200% of nondrizzling segments. We conclude that mesoscale and global circulation models stand to benefit greatly from the use of vertically dependent subgrid cloud parameterizations for both drizzling and nondrizzling stratocumulus clouds.

6. Acknowledgments

This study was supported by the National Weather Center Research Experiences for Undergraduates program through NSF Grant 0097651, and by the Environmental Sciences Division of the U. S. Department of Energy (through Battelle PNR Contract 144880-A-Q1 to the Cooperative Institute for Mesoscale Meteorological Studies) as part of the Atmospheric

Radiation Measurement Program, and the ONR Grants N00014-96-1-0687 and N00014-03-1-0304. Data were obtained from the Atmospheric Radiation Measurement (ARM) Program sponsored by the U.S. Department of Energy, Office of Science, Office of Biological and Environmental Research, Environmental Sciences Division. Special thanks to Daphne S. Zaras for the coordination of this program and the opportunities presented therein. The first author also thanks mentors Yefim L. Kogan and David B. Mechem for direction on this project and help along the way.

7. References

- Cahalan, R. F., Ridgway, W., Wiscombe, W. J., Bell, T. L., and J. B. Snider, 1994: The albedo of fractal stratocumulus. *J. Atmos. Sci.*, **51**, 2434-2460.
- Clothiaux, E. E., T. P. Ackerman, G. G. Mace, K. P. Moran, R. T. Marchand, M. A. Miller, and B. E. Martner, 2000: Objective determination of cloud heights and radar reflectivities using a combination of active remote sensors at the ARM CART sites. *J. Appl. Meteor.*, **39**, 645-665.
- Flynn, C., 2004a: Micropulse lidar (MPL) handbook. ARM Tech. Rep. ARM TR-019. 10pp.
- , 2004b: Vaisala ceilometer (model CT25K) handbook. ARM Tech. Rep. ARM TR-020, 19pp.
- , 2005: Belfort laser ceilometer (BLC) handbook. ARM Tech. Rep. ARM TR-040. 23pp.
- Kogan, Z. N., D. B. Mechem, and Y. L. Kogan, 2005: Assessment of variability in continental low stratiform clouds based on observations of radar reflectivity. *J. Geophys. Res.*, in press.
- Kogan, Y. L., 1998: Parameterization of cloud physics processes in mesoscale models of stratocumulus cloud layers, Preprints, *AMS Conference on Cloud Physics*, Everett, WA, Amer. Meteor. Soc., 348-351.

- Larson, V. E., R. Wood, P. R. Field, J. Golaz, T. H. Vonder Haar, and W. R. Cotton, 2001a: Systematic biases in the microphysics and thermodynamics of numerical models that ignore subgrid-scale variability. *J. Atmos. Sci.*, **58**, 1978-1994.
- , —, —, —, —, and —, 2001b: Small-scale and mesoscale variability of scalars in cloudy boundary layers: one-dimensional probability density functions. *J. Atmos. Sci.*, **58**, 1978-1994.
- Larson, V. E., J. Golaz, and W. R. Cotton, 2002: Small-scale and mesoscale variability of scalars in cloudy boundary layers: joint probability density functions. *J. Atmos. Sci.*, **59**, 3519-3539.
- Lhermitte, R. M., 1966: Probing air motion by Doppler analysis of radar clear air returns. *J. Atmos. Sci.*, **23**, 575-591.
- Mace, G. G., and K. Sassen, 2000: A constrained algorithm for retrieval of stratocumulus cloud properties using solar radiation, microwave radiometer, and millimeter cloud radar data. *J. Geophys. Res.*, **105**, 29 099-29 108.
- Moran, K. P., B. E. Martner, M. J. Post, R. A. Kropfli, D. C. Welsh, and K. B. Widener, 1998: An unattended cloud-profiling radar for use in climate research. *Bull. Amer. Meteor. Soc.*, **79**, 443-455.
- Pincus, R., and S. A. Klein, 2000: Unresolved spatial variability and microphysical process rates in large-scale models. *J. Geophys. Res.*, **105**, 27 059-27 065.
- Price, J. D., 2001: A study of probability distributions of boundary-layer humidity and associated errors in parametrized cloud-fraction. *Q. J. R. Meteorol. Soc.*, **127**, 739-758.
- Price, J. D., and R. Wood, 2002: Comparison of probability density functions for total specific humidity and saturation deficit humidity, and consequences for cloud parametrization. *Q. J. R. Meteorol. Soc.*, **128**, 2059-2072.

- Ramanathan, V., R. D. Cess, E. F. Harrison, P. Minnis, B. R. Barkstorm, E. Ahmad, and D. Hartman, 1989: Cloud-radiative forcing and climate: Results from the earth radiation budget experiment. *Science*, **243**, 57-63.
- Randall, D. A., J. A. Coakley, Jr., C. W. Fairall, R. A. Kropfli, and D. H. Lenschow, 1984: Outlook for research on subtropical marine stratiform clouds. *Bull. Amer. Meteor. Soc.*, **65**, 1290-1301.
- Rotstayn, L. D., 2000: On the “tuning” of autoconversion parameterizations in climate models, *J. Geophys. Res.*, **105**, 15 495-15 507.
- Sauvageot, H., and J. Omar, 1987: Radar reflectivity of cumulus clouds. *J. Atmos. Oceanic Technol.*, **4**, 264-272.
- Stokes, G. M., and S. E. Schwartz, 1994: The Atmospheric Radiation Measurement (ARM) program: Programmatic background and design of the cloud and radiation test bed. *Bull. Amer. Meteor. Soc.*, **75**, 1201-1221.
- Wang, J., and B. Geerts, 2003: Identifying drizzle within marine stratus with W-band radar reflectivity. *Atmos. Res.*, **69**, 1-27.
- Wood, R., P. R. Field, W. R. Cotton, 2002: Autoconversion rate bias in stratiform boundary layer cloud parameterizations. *Atmos. Res.*, **65**, 109-128.

8. Figure Captions

Figure 1. Histogram showing distribution of data as a function of segment length in hours. Number of segments are shown versus their length in hours.

Figure 2. Standard deviation of mean segment reflectivity (dBZ) plotted against the mean subcloud reflectivity (dBZ) at four levels: subcloud, base, middle, and top.

Figure 3. As in Figure 2, except in separate layer plots with polynomial curve fits. Levels follow: (a) subcloud, (b) base, (c) middle, and (d) top.

Figure 4. As in Figure 2, except data are plotted as polynomial curves without raw data.

Figure 5. Standard deviation of mean segment reflectivity (dBZ) plotted against the mean reflectivity at each level (dBZ). The four levels are: subcloud, base, middle, and top.

Figure 6. Sigma-bar, as defined in section 3a, Eq. 3 (dBZ), plotted against the mean subcloud reflectivity (dBZ). Bars show delta as defined in section 3a, Eq. 2.

Figure 7. Histogram showing the number of min/max standard deviation occurrences at each of the four levels: subcloud, base, middle, and top.

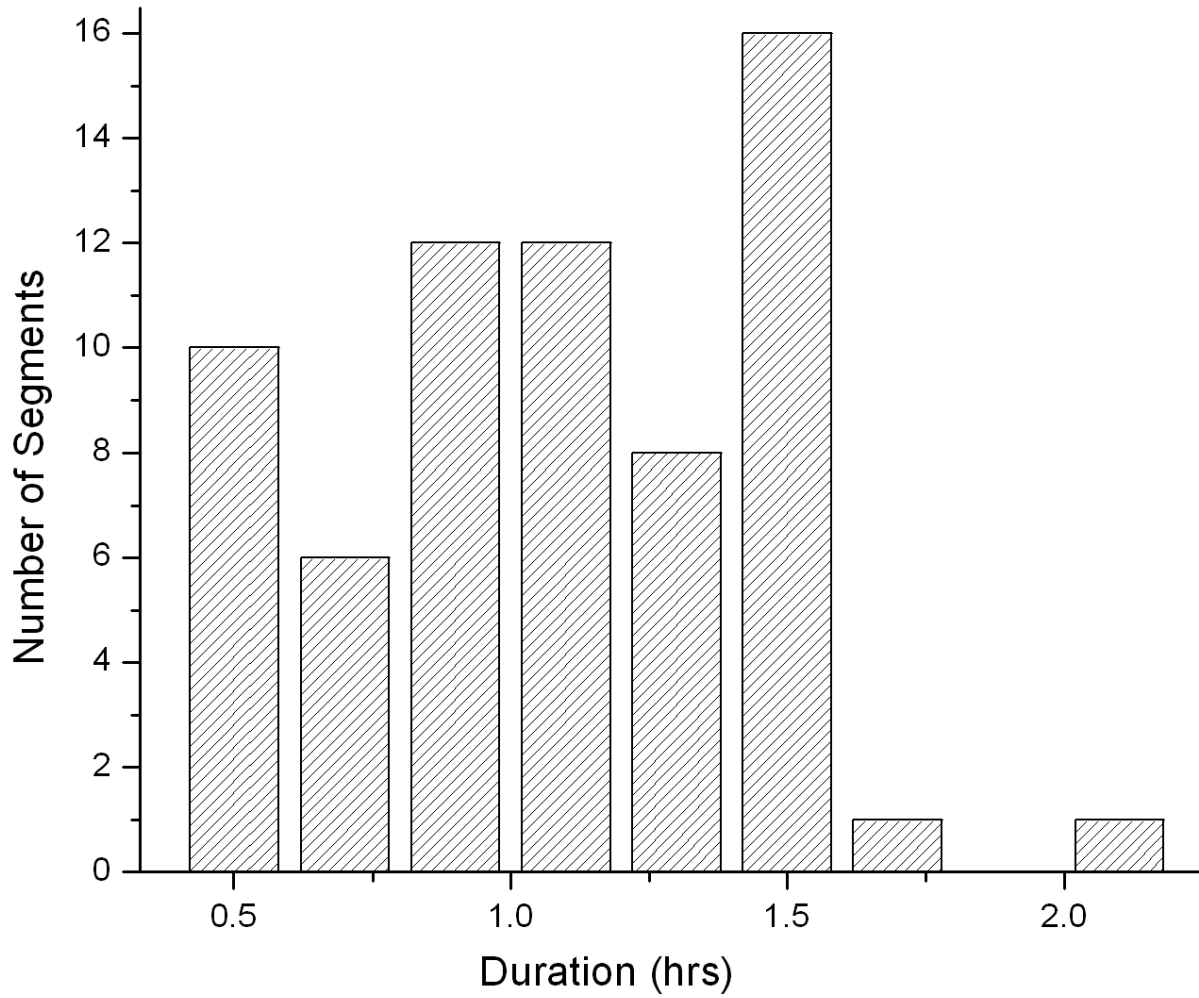


Figure 1. Histogram showing distribution of data as a function of segment length in hours. Number of segments are shown versus their length in hours.

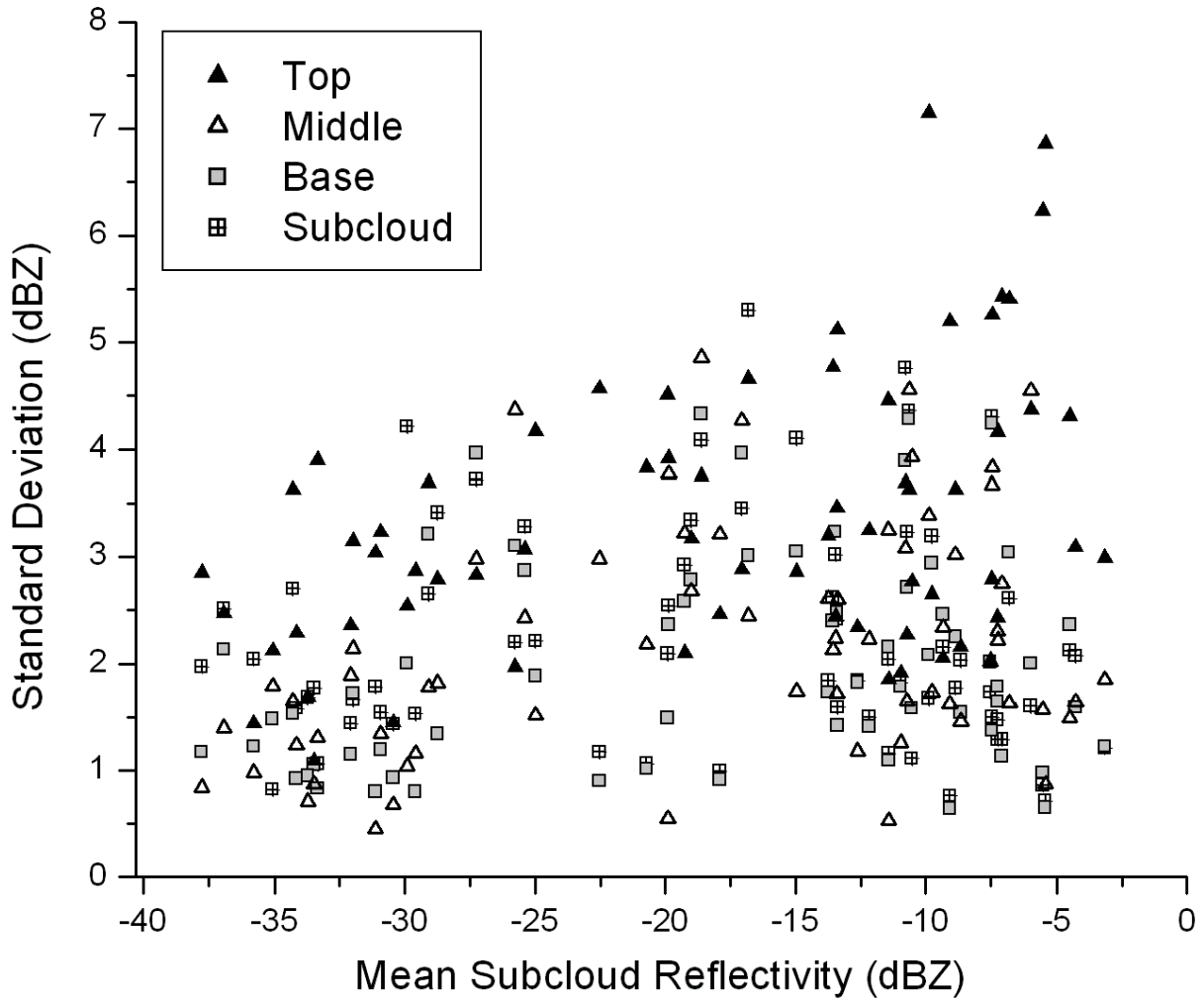


Figure 2. Standard deviation of mean segment reflectivity (dBZ) plotted against the mean subcloud reflectivity (dBZ) at four levels: subcloud, base, middle, and top.

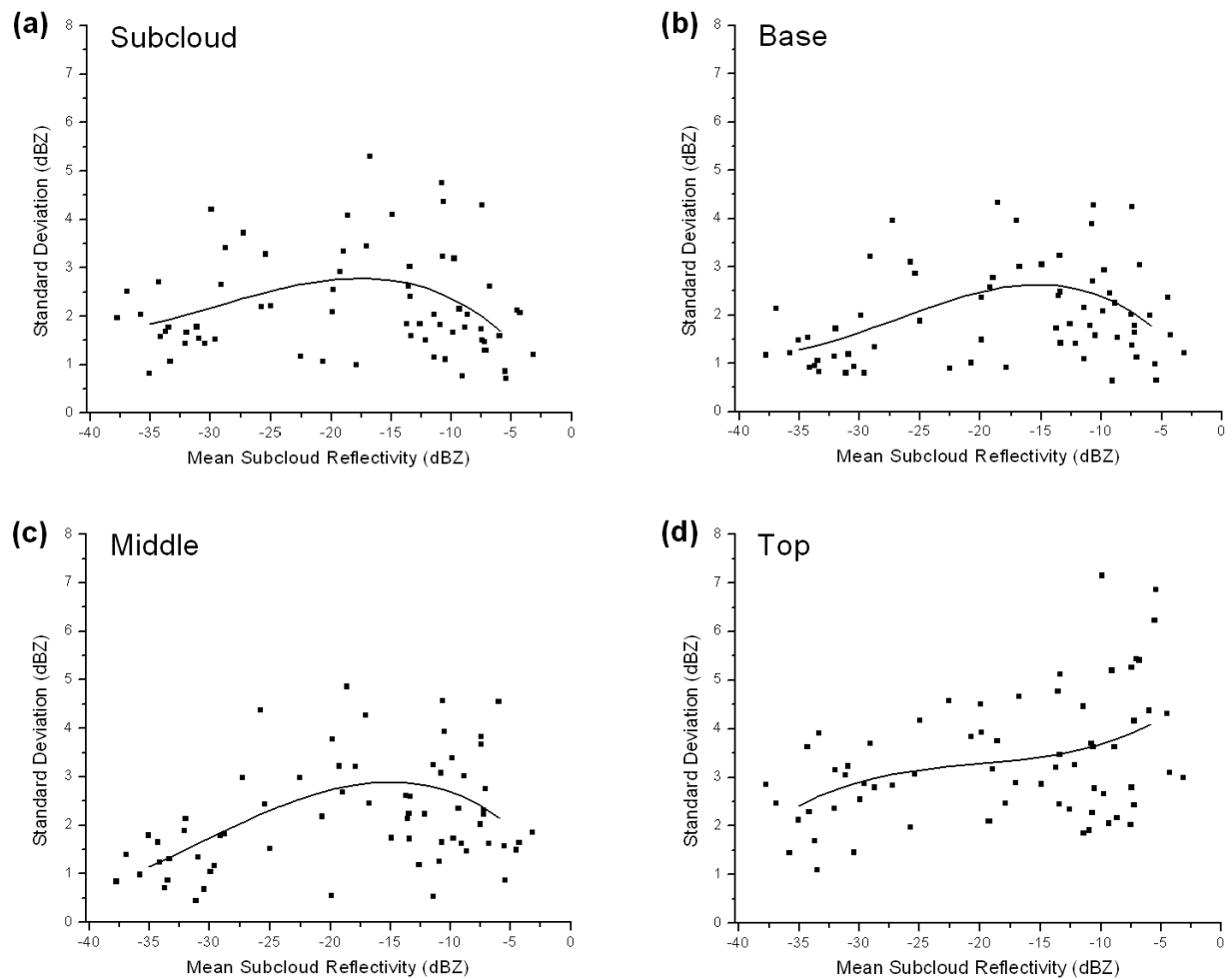


Figure 3. As in Figure 2, except in separate layer plots with polynomial curve fits. Levels follow: (a) subcloud, (b) base, (c) middle, and (d) top.

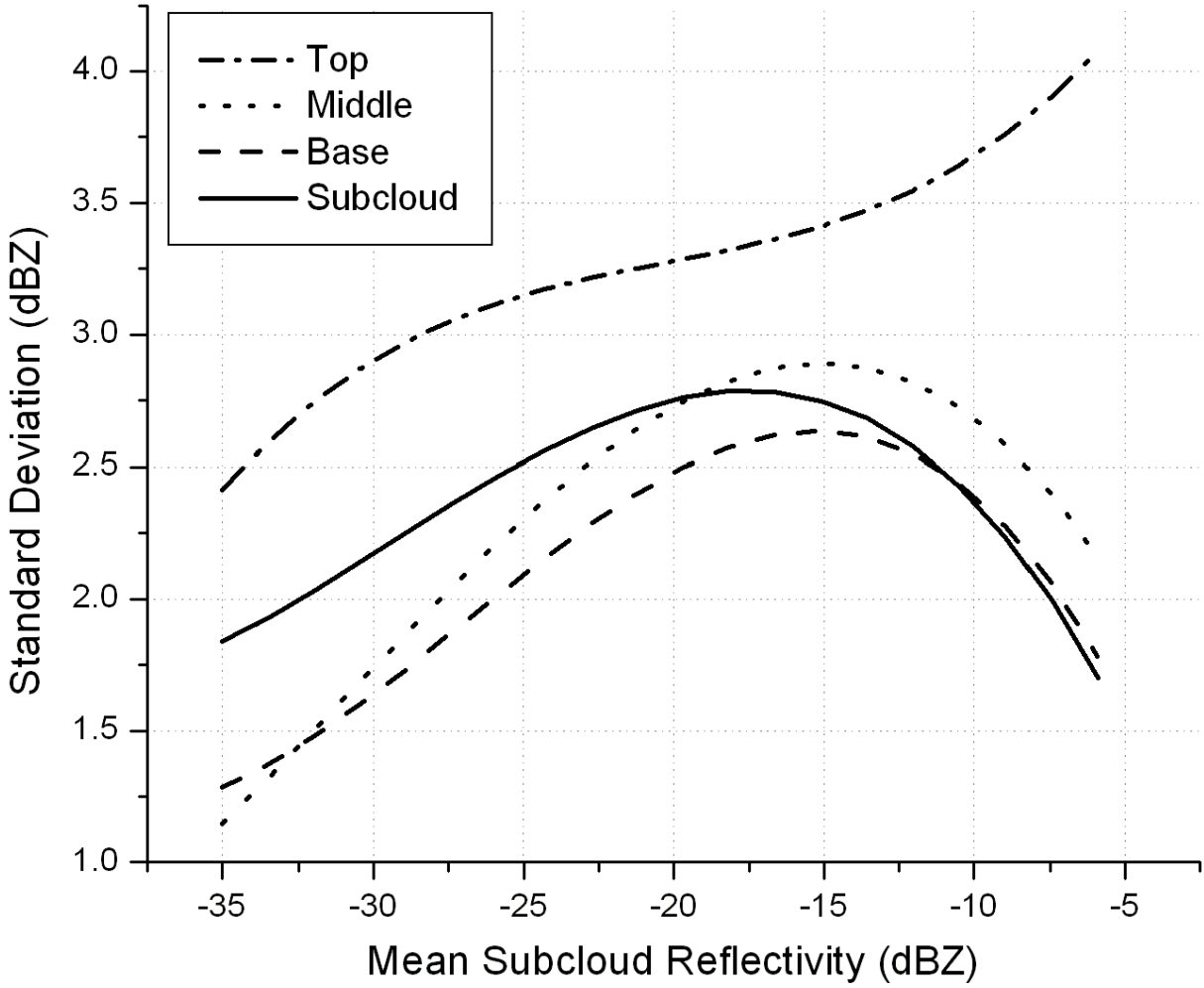


Figure 4. As in Figure 2, except data are plotted as polynomial curves without raw data.

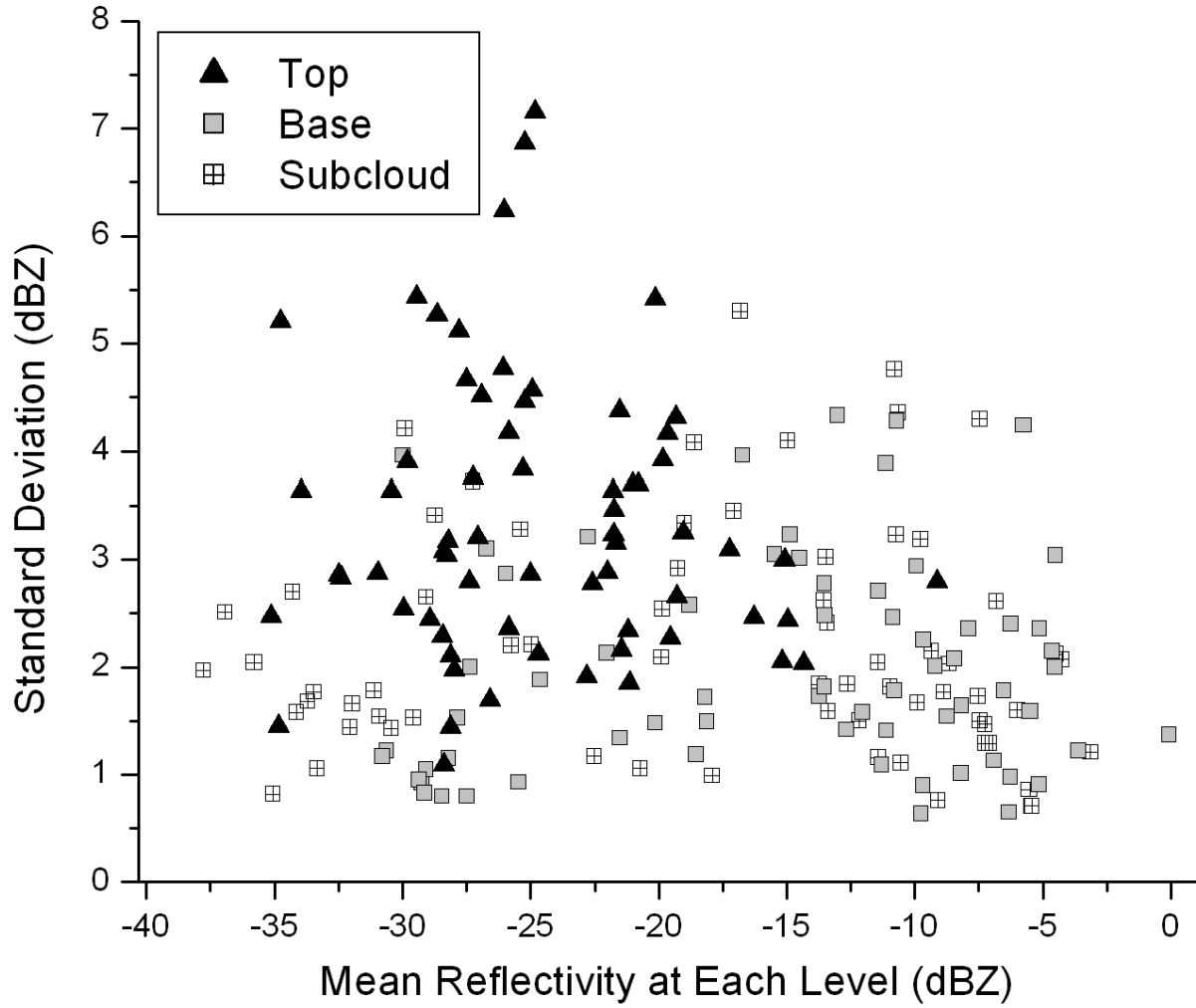


Figure 5. Standard deviation of mean segment reflectivity (dBZ) plotted against the mean reflectivity at each level (dBZ). The four levels are: subcloud, base, middle, and top.

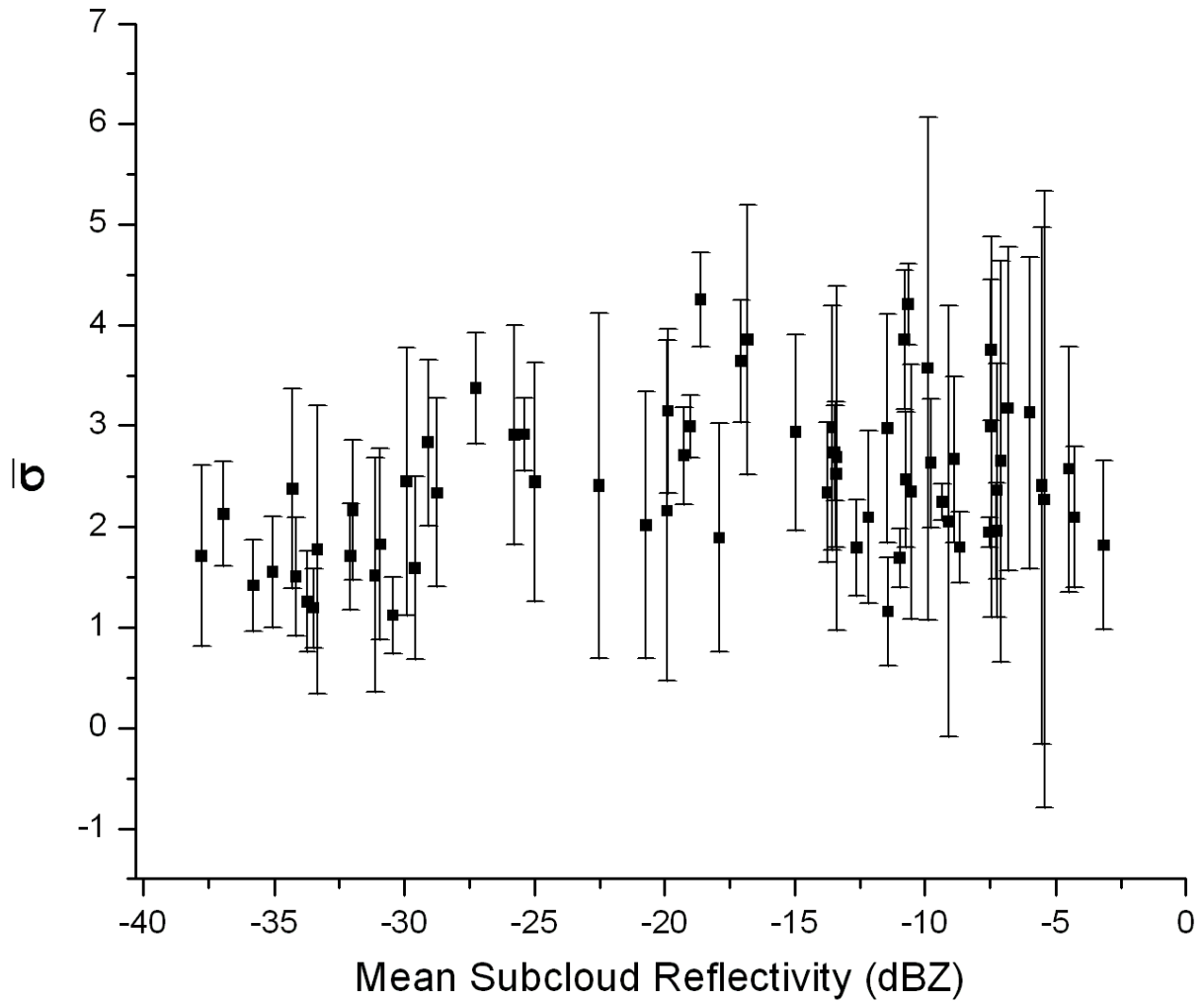


Figure 6. Sigma-bar, as defined in section 3a, Eq. 3 (dBZ), plotted against the mean subcloud reflectivity (dBZ). Bars show delta as defined in section 3a, Eq. 2.

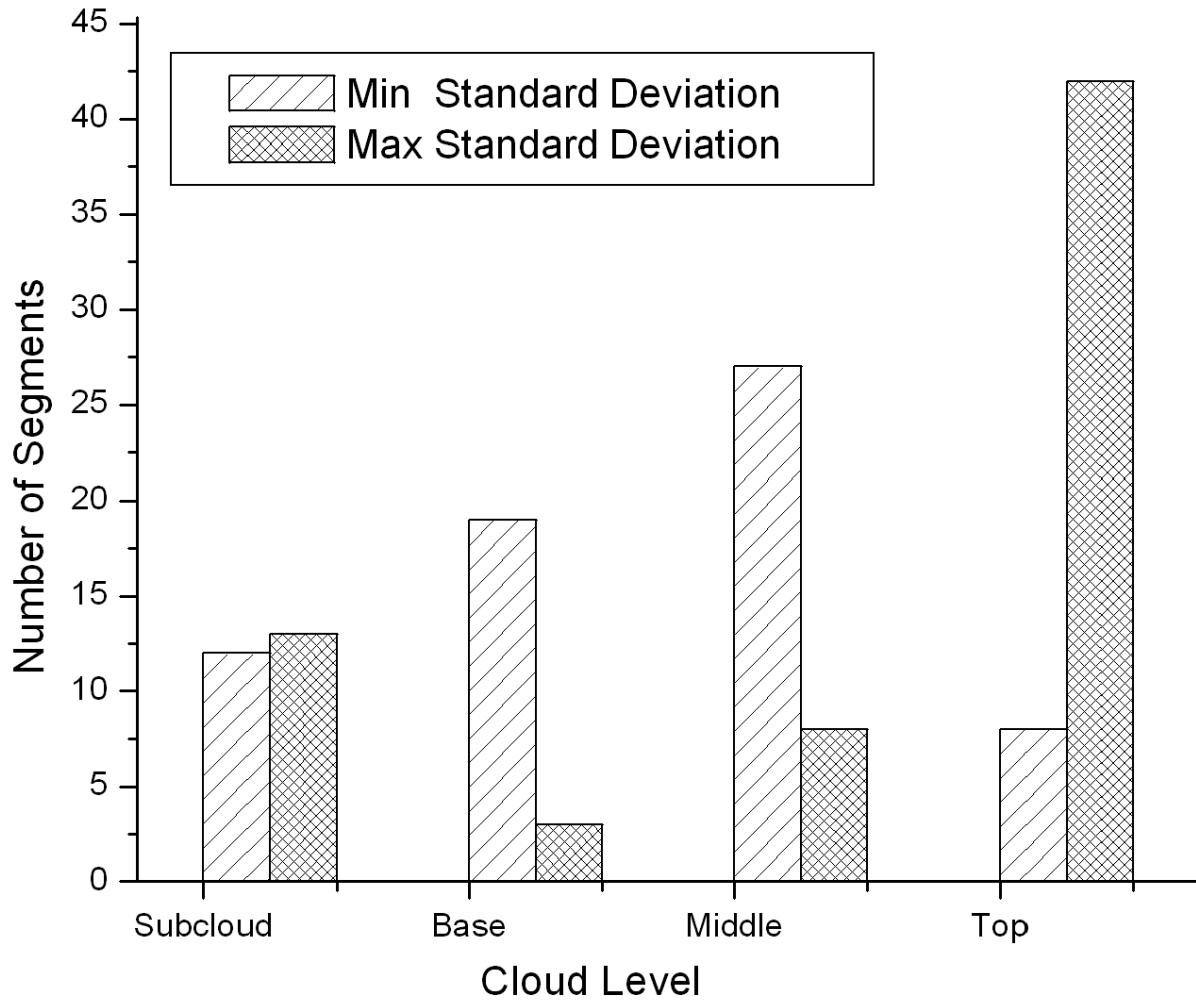


Figure 7. Histogram showing the number of min/max standard deviation occurrences at each of the four levels: subcloud, base, middle, and top.